DOI: 10.61782/fa.2025.0580

FORUM ACUSTICUM EURONOISE 2025

MODELLING OF THE ACOUSTIC EMISSION (AE) WAVE PROPAGATION USING THE AE TRANSMITTING SENSORS' RESPONSES

Van-Duong LE [1, 2*] **Marianne PERRIN** [1, 3] **Luis ESPINOSA** [1, 3]
Marie-Laetitia PASTOR [1, 3] **Yannick LE MAOULT** [4]
[1] University of Toulouse, Institut Clément Ader, CNRS 5312, IMT Mines Albi, INSA, ISAE-SUPAERO, UPS, 1 rue Lautréamont, 65000 Tarbes, France.
[2] The University of Danang - University of Science and Technology, 54 Nguyen Luong Bang, 550000 Danang, Viet Nam.
[3] Institut Universitaire de Technologie of Tarbes, Université de Technologie Tarbes Occitanie Pyrénées UTTOP, 65000 Tarbes, France.
[4] University of Toulouse, Institut Clément Ader, CNRS 5312, IMT Mines Albi, INSA, ISAE-SUPAERO, UPS, Campus Jarlard, Albi Cedex 09, 81013, France.

ABSTRACT[*]

Acoustic Emission (AE) testing is a non-destructive evaluation technique widely used in numerous fields providing ongoing monitoring to detect and track early signs of damage within structures. To ensure an effective interpretation of AE signatures in relation to damage mechanisms, a combination of numerical and experimental approaches is crucial for a comprehensive study of the measurement chain, including excitation sources, propagation mediums, sensors, acquisition systems and signal processing. This study aims to model the AE measurement chain using highly reproducible and reliably characterized emission waves from a piezoelectric sensor. To achieve this, the first step was to calibrate the source using a laser vibrometer. The aperture effect and several parameters of the sensor responses were investigated. Then, 3D models incorporating these source mechanisms within a metallic material were developed simultaneously by experiment and simulation to analyze AE wave propagation and measurement chain effects. Validated results in time and frequency domains showed good agreement, demonstrating the accuracy of the numerical approaches. These findings are crucial for gaining a significant understanding of AE sensors, contributing to sensor calibration processes, modelling of the entire measurement chain to enhance the interpretation of damage mechanisms.

Keywords: *Non-Destructive Evaluation (NDE), Acoustic Emission (AE), AE simulation, AE transmitting sensor, Aperture effect.*

1. INTRODUCTION

Non-Destructive Evaluation (NDE) techniques are widely used in numerous industrial fields to assess structural health and detect early damage without causing permanent harm of components and structures. These techniques provide inspections that are both safe and reliable, while remaining cost-effective and able to be conducted without interrupting ongoing operations. Acoustic Emission (AE) method is one of the most frequently employed NDE methods to detect and track early signs of damage in mechanically loaded structures and components. In such cases, the AE waves are generated by the sudden releasing of energy under the form of elastic waves and propagating in all directions within the material. The source of AE events may come from natural phenomena (earthquakes, rock bursts) [1], deformation

[*]***Corresponding author**: vanduong.le@iut-tarbes.fr*

processes [2], crack propagation [3], damage mechanisms in composite structure [4], etc. These AE waves are usually captured by sensors which convert the mechanical disturbance on the contact surface into a voltage-time waveform signal, providing information about the location and characteristics of AE events. The detection process of AE signals is described by the measurement chain illustrated in Figure 1. According to this, an AE signal in time domain S(t) is obtained by the convolution (⊗) of the characteristics of all elements in the measurement chain, from excitation source F(t), propagation medium G(t), coupling conditions C(t) and sensor transfer function H(t), and acquisition system A(t) as Eqn. (1):

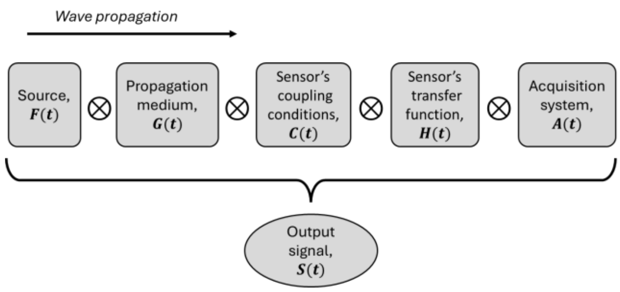

Figure 1. Measurement chain used for detection of AE waves.

$$S(t) = F(t) \otimes G(t) \otimes C(t) \otimes H(t) \otimes A(t) \quad (1)$$

The main scientific obstacles in enhancing our understanding of AE results lies in comprehending how the signal evolves from the excitation source to the obtained signal that highly dependent on the measurement chain configurations, such as excitation source mechanisms [5-6], structure and material properties, observation distance and direction [12-14], and sensors characteristics and its coupling conditions [15]. Piezoelectric sensors are widely used in AE testing due to their high sensitivity and affordability; however, their transfer function varies significantly based on sensor type, structure, and operating frequency [16-17]. These significant influences of the measurement chain configuration lead greater challenges when determining a robust correlation between AE signal characteristics and their respective actual excitation mechanisms. Addressing these challenges requires a well-defined characterization of each element in the measurement chain, which can be achieved through an effective combination of numerical and experimental approaches. For this purpose, studies should be carried out with configurations that include well-defined source mechanisms and propagation medium properties, facilitating a more straightforward analysis of the other elements in the measurement chain. With the rapid advancements in science and technology, numerical simulation tools have become essential and widely used by researchers to analyze the complex interactions and propagation of AE waves. Several mechanisms, simplified from AE events, have been used in simulations involving changes in applied force, displacement, or released energy over a very short excitation time. For instance, pencil-lead breaks sources are used to validate numerical results against experimental data, supporting the modeling of conical sensors, and considering the influence of geometrical specimen on AE signal characteristics [8, 18]. Moreover, glass tube fracture sources have been modeled and applied in research calibration processes for AE sensors [10, 16]. The mechanical impact sources are used to investigate the boundary reflection conditions and sensor characteristics in detecting AE wave propagation [19]. Another AE source mechanism consists of using a laser to generate an ultrasonic excitation that was used to obtain the calibration curve of piezoelectric sensors [20]. Furthermore, an artificial source generated by an AE sensor directly excited by an electrical pulse is also used in numerical research to study the complex behavior of piezoelectric conversion in AE sensors, as well as the influence of factors related to the propagation mediums of AE waves [14, 21]. Compared to other sources, the one generated by transmitting sensors offers higher reproducibility through control of the electrical pulse configuration, while also facilitating a better understanding of the electrical-mechanical conversion process, known as the sensor's response, thus contributing to successful sensor modeling in numerical approaches. The sensor's response is influenced not only by the sensor's geometry and the spatial variations across the sensor surface but also on the operating frequency, known as aperture effect [7, 21-22]. To the best of our knowledge, there has been limited exploration in literature regarding the precise determination of the response of transmitting sensors and its application in numerical studies to examine the influence of the AE measurement chain.

In this study, the source mechanism from AE sensors in terms of the normal velocity response was first characterized by using a laser vibrometer. Two types of sensors were used, including a resonant sensor, R15α, and a wideband sensor, F15α (from Physical Acoustics, USA). The influences of aperture effect on the response of each sensor were investigated. Next, 3D models incorporating these mechanisms were developed to study the wave propagation and the influence of the measurement chain. The simulation results were validated with experiments to verify the accuracy of the modelling parameters and setup. Finally, the impact of contact surface conditions on the amplitude of the sensor response was taken into account to enhance the accuracy of the simulation results.

2. MEASUREMENT OF THE SENSOR'S RESPONSE

The vibration velocity responses across the active surface of sensors are non-uniform due to the aperture effect. To demonstrate this, a simplified model of the velocity response assumes that the variation across different positions on the sensor surface can be represented by the maximal velocity response usually measured at the center region of the surface, $v_{center}(t)$, multiplied by a k parameter as shown in Eqn. (2) [7].

$$v(t) = \frac{1}{S} \iint_S k(r).v_{center}(t)\, dS \tag{2}$$

Where S denotes the contact surface area of sensor, $k(r)$ is called the aperture effect function of the sensor and is a real number ranging from 0 to 1. This parameter represents the sensitivity of the normal vibration velocity at a position located at radius r, relative to its value at the center region of the sensor surface. In this study, two types of AE sensors were utilized: the narrowband resonance sensor, type R15α, with an operating frequency range from 50 kHz to 400 kHz, and the wideband flat frequency sensor, type F15α, with an operating frequency range from 100 kHz to 450 kHz.

Figure 2 shows the setup of the testing for measuring AE sensor response in terms of normal vibration velocity on its active surface. The acquisition includes an OFV-505 sensor head connected to an OFV-5000 vibrometer controller which was set with a VD-09 decoder board, and bandpass filter from 100 Hz to 1 MHz adapted to AE wave characteristics [1]. Ultrasonic excitation was obtained using a UTC110 system (MISTRAS, France), controlled through the EuroScan V software. AE sensors were fixed on a displacement system by plastic clamping units. The measurements on the active surface of the sensors were conducted along the centerline with a spacing of 200 µm between each point. The experimental data from the tests were processed using MATLAB® with a 4th-order Butterworth low-pass filter as in [18], with a cutoff frequency of 500 kHz adapted to operating frequency ranges of used sensors.

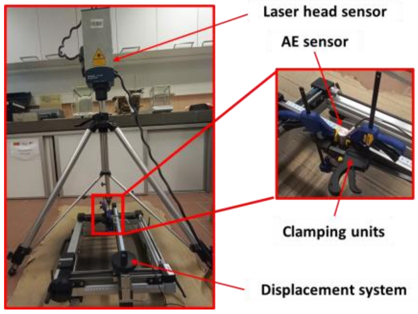

Figure 2. Test layout for measuring sensor's response in term of normal vibration velocity.

3. 3D MODELS OF WAVE PROPAGATION

3D models incorporating source mechanisms generated by transmitting sensors' response were established simultaneously by experiment and simulation as shown in Figure 3 a, and b, respectively. In the case of experiment, the same acquisition system as previous measurements were used to capture normal velocity of AE waves within an aluminum plate of dimensions 500 mm x 500 mm x 2mm. The AE sensor was mounted on the specimen surface by a thin layer of silicon glue. After several tests to determine the optimal excitation parameters, an excitation pulse with 100 volts and a rise time of 700 ns was applied to the AE sensor. The signals were obtained at two positions located at 30 mm and 90 mm as distances from sensors. A finite element approach was conducted by using the software COMSOL Multiphysics® through module "Solid Mechanics (Elastic waves)". The setup includes a 3D aluminum plate dimensioning 250 x 300 x 2 mm with its properties referred to [8]. The low-reflection conditions were applied to minimize the effects of reflected waves adapted to free conditions of wave propagation in larger geometry as experimental condition. The source from transmitting sensors were set on its contact surface using velocity response according to Eqn. (2) based on experimental results. Several tests were performed to determine the convergence of mesh element size and critical timestep. Based on these findings, the element size of 1 mm, corresponding timestep of 0.15 µs were chosen, offering a good compromise with computational time. On the other hand, a linear combination of mass and stiffness matrices were applied considering the attenuation of wave amplitude during propagating. Here, α and β are the mass and stiffness proportionality coefficients, as known as Rayleigh damping coefficients. Both AE sensors used with operating frequency range less than 500 kHz, so the impact of β (mostly in high frequency) is neglected. Only α is applied (in low frequency), set to 30000, adapting with a damping factor of 0.002 at maximum frequency of 1 MHz based on experimental results.

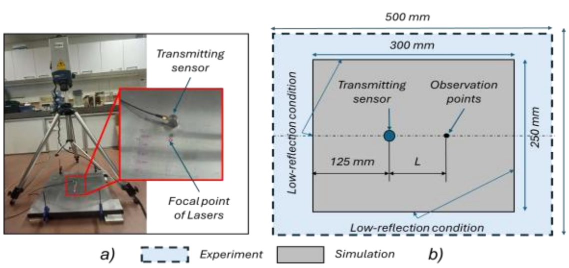

Figure 3. 3D models of wave propagation used for experiment (a) and simulation (b).

4. RESULTS AND DISCUSSION

4.1 Sensor surface velocity response and aperture effects

4.1.1 Sensor velocity response of sensors

The results in the response of two sensors at the surface center in terms of normal vibration velocity are illustrated in Figure 4. The normal velocity response varies significantly depending on the sensor type, affecting both waveform and its amplitude. The R15α resonant sensor shows higher sensitivity in peak velocity compared to the F15α wideband sensor, measuring 4.5 mm/s and 3.4 mm/s, respectively. Due to the inherent characteristics of resonant sensors, the R15α can maintain oscillations with minimal excitation energy, resulting in extended signal retention and higher amplitude responses compared to the F15α sensor.

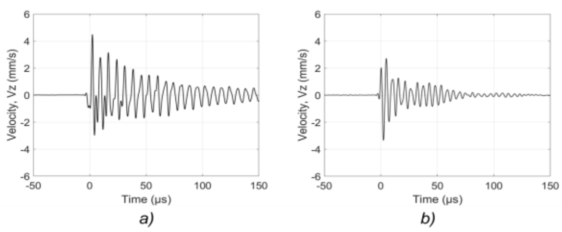

Figure 4. The velocity response measured at the center of surface for R15α (a) and F15α (b) sensors.

4.1.2 Peak velocity response across entire sensor surface

Figure 5 shows the results of peak velocity response across full measured diameter on active surface of both sensors. The standard deviation of peak velocity across 32 consecutive measurements remained below 0.1 mm/s (less than 3% of the max values) in most cases, demonstrating high reliability of tests. It can observe that the obtained peak velocity tends to exhibit symmetry along the centerline of the sensor's active surface. The results indicate that the peak velocity response varies with position on the sensor's contact surface, with higher values at the central region and decreasing towards the edges, depending on the sensor type. This is consistent with previous tests conducted on the μ80 sensor [22]. These findings highlight the influence of the aperture effect on the response of the AE sensors.

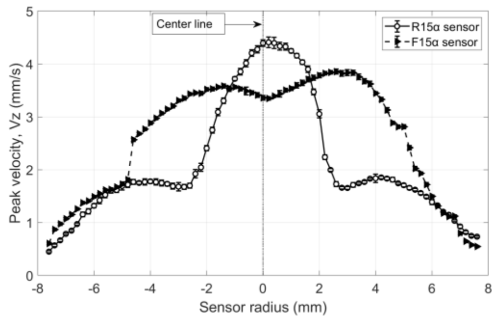

Figure 5. Peak normal velocity of the sensor response measured by laser vibrometer.

4.1.3 Aperture effect function of sensors

The *k(r)* factor, representing the influence of the aperture effect (Eqn. (2)), is illustrated in Figure 6. The analysis focuses on half of the sensor surface, taking into account its symmetrical response along the centerline. Here, the *k(r)* values were determined by normalizing the peak velocity at a given position *r* with respect to the maximum peak velocity response measured at the central region, followed by smoothing using a Savitzky-Golay filter [23]. For the R15α sensor, the highest *k(r)* value was found at the center, gradually decreasing toward edges of the sensor. Conversely, the F15α sensor exhibited a more uniform distribution, with *k(r)* values ranging between 0.93 and 1 over a central region extending up to 4 mm. These findings indicate that the peak amplitude variation across the sensor surface does not follow a simple uniform decay, as previously assumed [7], but rather depends on both sensor characteristics and radial position *r*. The observed variations can be attributed to the aperture effect, which influences the sensor's transmitting transfer function, with dependencies on spatial positioning and operating frequency [7, 21-22]. This study enhances the understanding of how AE sensors convert electrical excitation into mechanical vibrations, providing valuable insights into source identification using transmitting sensors, contributing directly to accurate numerical sensor modeling, and the characterization of AE sensor transfer functions.

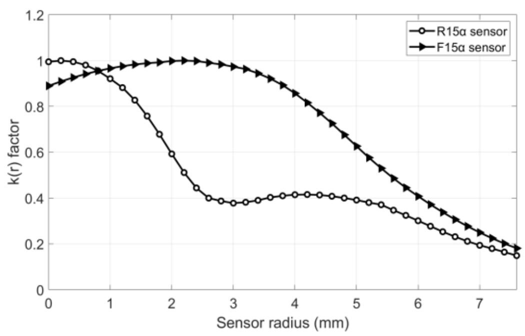

Figure 6. The values of *k(r)* as aperture effect function for both sensors.

4.2 AE wave propagation modelling

4.2.1 Excitation source mechanisms caused by AE sensors

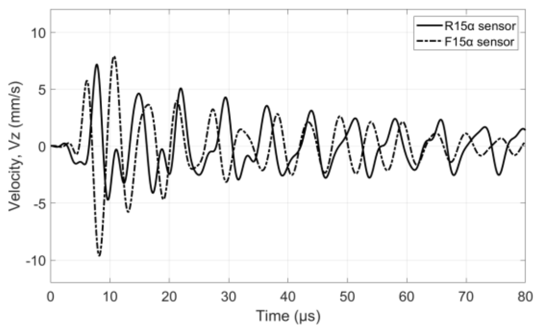

Figure 7. Source mechanisms generated by AE sensor response applying to numerical models.

The excitation source mechanisms generated by the transmitting sensor response for the R15α and F15α sensors are illustrated in Figure 7. These results were calculated using Eqn. (2), considering the sensor response at the center of the surface and its aperture function, which were applied for simulation.

4.2.2 Comparison of experimental and numerical results in both time and frequency domains

To match the configuration of the laser vibrometer in the testing setup, a 4th-order Butterworth bandpass filter (100 Hz – 1 MHz) was applied to the numerical results. Validation was performed by comparing the simulated and experimental normal velocity waveforms in the time domain and their corresponding FFTs, as shown in Figures 8 and 9, respectively, at observation points 30 mm and 90 mm away. Overall, the results show strong agreement across both domains. In order to quantify this agreement, the Pearson's correlation coefficient [24-25] was calculated for the full signal duration, a 30 μs window from the onset (limited between two vertical dash line), and the FFT results, summarized in Table 1. It is noted that a maximum correlation coefficient of 1 indicates a perfect positive correlation, -1 represents a perfect negative correlation, and 0 indicates no correlation. In all cases, the correlation coefficient ranged from 0.61 to 0.8 for the full signal, from 0.56 to 0.78 for the 30 μs window, and remained around 0.85 for the FFT results. These values align well with previous studies on AE wave modeling from pencil-lead breaks [9, 43]. A slight discrepancy in peak velocity was observed for the F15α sensor, with a difference of 1.3 mm/s at 30 mm and 0.3 mm/s at 90 mm, while for R15α sensor it is negligible. In the frequency domain, the R15α sensor results closely matched in both peak frequency and magnitude, while the F15α sensor showed a deviation of approximately 35 kHz and 10 dB, respectively. These differences might be caused by variations in sensor contact conditions during measurements and validation, as previously discussed in [21] and further discussions in the final section. A strong agreement between the experimental and simulation results validated the accuracy of the proposed numerical model, the calibrated excitation source mechanism from the transmitting sensors' responses and its aperture effect, and its application to AE wave propagation.

Table 1. Summary of the correlation coefficients of validated results.

Sensors	R15α		F15α	
Positions	30 mm	90 mm	30 mm	90 mm
Full duration	0.61	0.8	0.63	0.62
Within 30 μs	0.56	0.78	0.73	0.72
FFT	0.86	0.86	0.85	0.84

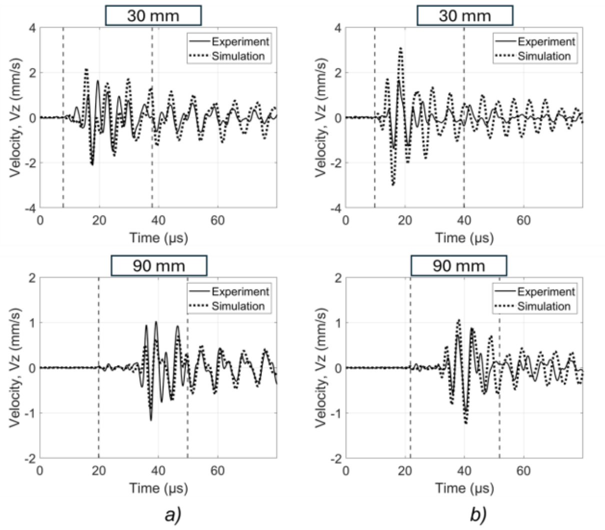

Figure 8. Validated results for the normal velocity of AE wave propagation generated by the response of R15α (a) and F15α (b) sensors.

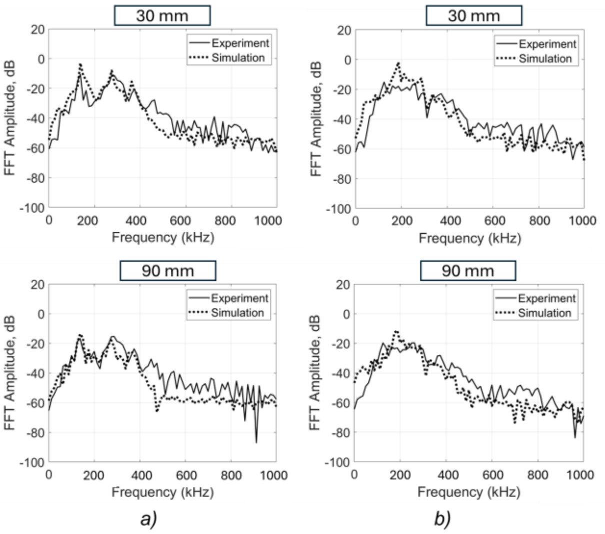

Figure 9. Validated results for FFT transformation of the AE wave propagation generated by response of R15α (a) and F15α (b) sensors. For vertical axis, 0 dB is referenced at 1 V/(mm/s).

4.2.3 . Consideration of the influence of sensor contact conditions

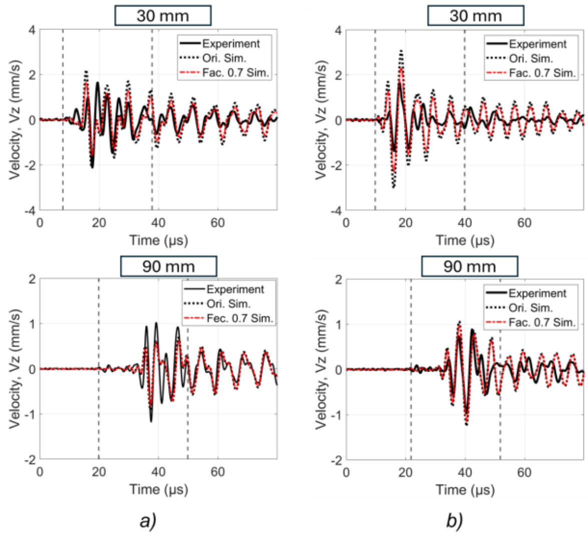

Figure 10. Validated results of normal velocity signals, accounting for the influence of the loss factor due to different sensor surface contact conditions, for R15α (a) and F15α (b) sensors.

As mentioned previously, differences in sensor's contact conditions may explain the slightly higher peak velocity and FFT magnitude observed in the simulation compared to the experiment in the near field. In sensor response measurements, the transmitting sensor's active surface was in free contact with air, whereas in the validation tests, it was in loaded contact with the specimen surface through a thin layer of silicon glue. In free contact conditions, the large impedance mismatch between the sensor and air could lead to increased oscillation energy at the surface, potentially enhancing resonance effects. In contrast, under loaded contact conditions, the smaller impedance mismatch, along with the applied pressure and coupling, resulted in smoother vibrations with lower amplitudes [21]. To account for the reduction in sensor response amplitude due to contact condition changes, a constant correction factor was introduced to improve simulation accuracy. Numerical simulations were conducted to evaluate the impact of different amplitude loss factors on the velocity response of transmitting sensors. The findings indicate that applying a loss factor of 0.7 improves agreement between simulated and experimental results. The damping coefficient α was recalculated and set to 12000 corresponding to the incorporating losing factor and its impact on the excitation source's maximum amplitude. The final normal velocity signals are presented in Figure 10, comparing the original simulation (black dotted line), the simulation with a 0.7 loss factor (red line), and the experimental results (solid black line). Applying the loss factor improved the alignment between simulation and experiment, with a maximum error below 0.5 mm/s for the F15α sensor, while maintaining similar accuracy for the R15α sensor.

5. CONCLUSION

In this study, the normal velocity response on the active surface of two types of piezoelectric AE sensors was analyzed: the R15α, a narrowband resonant sensor, and the F15α, a wideband sensor with a flat frequency response. Additionally, 3D models were developed to simulate AE wave propagation generated by the response of transmitting sensors within an aluminum plate. To begin with, the results indicated that the normal velocity response is not uniform across the sensor surface and decreases toward the edges of the surface. Resonant sensors exhibited higher energy, with maximum sensitivity concentrated in a small central region of the surface, whereas wideband sensors showed lower energy but distributed peak sensitivity over a broader area. The study further examined *k(r)* as a function of the aperture effect, emphasizing the effects of sensor geometry, spatial variations, and operating frequency in shaping the peak normal velocity response. These findings provide valuable insights into AE sensor behavior, enabling improved sensor modeling in numerical methods without requiring detailed physical geometry. On the other hand, a very good agreement was observed between simulation and experimental results in both time and frequency domains, validating the accuracy of the numerical approach. To address variations in sensor response amplitude due to different coupling conditions, a loss factor was introduced, refining the simulation accuracy by accounting for changes from free contact (air) to loaded contact (specimen surface). These results contribute to a more comprehensive understanding of signal transformation from the source mechanism through wave propagation to the acquisition system, supporting the development of an improved AE measurement framework.

6. REFERENCES

[1] P. Kundu, "Review of rotating machinery elements condition monitoring using acoustic emission signal," *Expert Systems with Applications*, vol. 252, pp. 124169, 2024.

[2] C. K. Tan, P. Irving, and D. Mba, "A comparative experimental study on the diagnostic and prognostic capabilities of acoustics emission, vibration and spectrometric oil analysis for spur gears," *Mechanical Systems and Signal Processing*, vol. 21, no. 1, pp. 208–233, 2007.

[3] M. Chai, X. Hou, Z. Zhang, and Q. Duan, "Identification and prediction of fatigue crack growth under different stress ratios using acoustic emission data," *International Journal of Fatigue*, vol. 160, p. 106860, 2022.

[4] P. J. de Groot, P. A. M. Wijnen, and R. B. F. Janssen, "Real-time frequency determination of acoustic emission for different fracture mechanisms in carbon/epoxy composites," *Composites Science and Technology*, vol. 55, no. 4, pp. 405–412, 1995.

[5] W. Roundi, A. El Mahi, A. El Gharad, and J.-L. Rebiere, "Acoustic emission monitoring of damage progression in Glass/Epoxy composites during static and fatigue tensile tests," *Applied Acoustics*, vol. 132, pp. 124–134, 2018.

[6] S. Masmoudi, A. El Mahi, and S. Turki, "Use of piezoelectric as acoustic emission sensor for in situ monitoring of composite structures," *Composites Part B: Engineering*, vol. 80, pp. 307–320, 2015.

[7] Z. Hamam, N. Godin, C. Fusco, and T. Monnier, "Modelling of Acoustic Emission Signals Due to Fiber Break in a Model Composite Carbon/Epoxy: Experimental Validation and Parametric Study," *Applied Sciences*, vol. 9, no. 23, 2019.

[8] T. Le Gall, T. Monnier, C. Fusco, N. Godin, and S.-E. Hebaz, "Towards Quantitative Acoustic Emission by Finite Element Modelling: Contribution of Modal Analysis and Identification of Pertinent Descriptors," *Applied Sciences*, vol. 8, no. 12, p. 2557, 2018.

[9] Z. Hamam, N. Godin, C. Fusco, A. Doitrand, and T. Monnier, "Acoustic Emission Signal Due to Fiber Break and Fiber Matrix Debonding in Model Composite: A Computational Study," *Applied Sciences*, vol. 11, no. 18, 2021.

[10] M. G. R. Sause and M. A. Hamstad, "Numerical modeling of existing acoustic emission sensor absolute calibration approaches," *Sensors and Actuators A: Physical*, vol. 269, pp. 294–307, 2018.

[11] R.-R. Naber and H. Bahai, "Analytical and experimental validations of a numerical band-limited Green's function approach for modelling

acoustic emission waves," *Advances in Engineering Software*, vol. 38, no. 11, pp. 876–885, 2007.

[12] Y. Wu, M. Perrin, M.-L. Pastor, P. Casari, and X. Gong, "On the determination of acoustic emission wave propagation velocity in composite sandwich structures," *Composite Structures*, vol. 259, pp. 113231, 2021.

[13] Y. Wu, M. Perrin, M.-L. Pastor, P. Casari, and X. Gong, "Moisture Effects on Acoustic Emission Characteristics and Damage Mechanisms of Balsa Wood Core Composite Sandwich under 4-Point Bending," *Materials*, vol. 17, no. 5, pp. 1044, 2024,

[14] T. I. Khan, A. A. Rashid, and T. Nanami, "Theoretical and experimental analysis of acoustic emission signal for resonant sensor on homogenous material," *Sensing and Bio-Sensing Research*, vol. 39, pp. 100550, 2023.

[15] C. Hellier, *Handbook of nondestructive evaluation*. New York: McGraw-Hill, 2003.

[16] G. C. McLaskey and S. D. Glaser, "Acoustic Emission Sensor Calibration for Absolute Source Measurements," *Journal of Nondestructive Evaluation*, vol. 31, no. 2, pp. 157–168, 2012.

[17] K. Ono, "Rayleigh Wave Calibration of Acoustic Emission Sensors and Ultrasonic Transducers," *Sensors*, vol. 19, no. 14, pp. 3129, 2019.

[18] M. G. R. Sause, M. A. Hamstad, and S. Horn, "Finite element modeling of conical acoustic emission sensors and corresponding experiments," *Sensors and Actuators A: Physical*, vol. 184, pp. 64–71, Sep. 2012.

[19] Z. Heidary and D. Ozevin, "On the Influences of Boundary Reflections and Piezoelectric Sensors to the Characteristics of Elastic Waves for Pattern Recognition Methods," *Journal of Nondestructive Evaluation*, vol. 34, no. 1, pp. 271, 2014.

[20] L. Zhang, H. Yalcinkaya, and D. Ozevin, "Numerical approach to absolute calibration of piezoelectric acoustic emission sensors using multiphysics simulations," *Sensors and Actuators A: Physical*, vol. 256, pp. 12–23, 2017.

[21] N. Boulay, A. Lhémery, and F. Zhang, "Simulation of the spatial frequency-dependent sensitivities of Acoustic Emission sensors," *Journal of Physics: Conference Series*, vol. 1017, pp. 012008, 2018.

[22] T. Monnier, S. Dia, N. Godin, and F. Zhang, "Primary Calibration of Acoustic Emission Sensors by the Method of Reciprocity, Theoretical and Experimental Considerations," *Journal of Acoustic Emission*, vol. 30, pp. 152–166, 2012.

[23] Abraham. Savitzky and M. J. E. Golay, "Smoothing and Differentiation of Data by Simplified Least Squares Procedures.," *Analytical Chemistry Journal*, vol. 36, no. 8, pp. 1627–1639, 1964.

[24] N. Godin, P. Reynaud, and G. Fantozzi, "Challenges and Limitations in the Identification of Acoustic Emission Signature of Damage Mechanisms in Composites Materials," *Applied Sciences*, vol. 8, no. 8, pp. 1267, 2018.

[25] T. Le Gall, "Simulation de l'émission acoustique : Aide à l'identification de la signature acoustique des mécanismes d'endommagement," These de doctorat, Lyon, 2016.